Available online at www.sciencedirect.com
ScienceDirect
Annals of Nuclear Energy 34 (2007) 424–432
annals of NUCLEAR ENERGY
www.elsevier.com/locate/anucene

Two-dimensional nodal transport method for triangular geometry

Haoliang Lu [a,*], Hongchun Wu [a], Liangzhi Cao [a], Yongqiang Zhou [a], Chunyu Xian [b], Dong Yao [b]

[a] Department of Nuclear Engineering, Xi'an Jiaotong University, Xi'an, Shaanxi 710049, China
[b] Nuclear Power Institute of China, Chengdu, Sichuan 610041, China

Received 4 April 2006; received in revised form 4 February 2007; accepted 9 February 2007
Available online 2 April 2007

Abstract

The advanced nodal method for solving the multi-group neutron transport equation in two-dimensional triangular geometry is developed. To apply the transverse integration procedure, an arbitrary triangular node is transformed into a regular triangular node using coordinate transformation. The angular distributions of intra-node neutron fluxes and its transverse-leakage are represented by the S_N quadrature set. The spatial distributions of neutron flux and source in the regular triangle are given approximately by an orthogonal quadratic polynomial, and the spatial expansion of transverse-leakage is approximated by a second-order polynomial. To establish a stable and efficient iterative scheme, the improved nodal-equivalent finite difference algorithm is used. The results for several benchmark problems demonstrate the higher capability of the method to yield the accurate results in significantly smaller computing times than those required by the standard finite difference method and the finite element spherical-harmonics method.

1. Introduction

Many methods, such as a finite element spherical harmonics method (McGhee et al., 1997; Cao and Wu, 2004), a discrete ordinates finite element method (Ressel and Starke, 2000) and an exponential characteristic method (Mathews and Brennan, 1997), have been developed for an accurate analysis of the neutron transport problems for the unstructured triangular meshes in the last decade. However, the computational cost of these methods is greater, especially for the problems needing the many meshes. The nodal transport method is widely accepted as the accurate and efficient analytical method for the problems of the light water reactors with the rectangular geometry (Badruzzaman, 1985) and the fast reactors with the hexagonal geometry (Wagner, 1989; Ikeda and Takeda, 1994). But to my knowledge, there is no nodal transport method can solve the problems with the unstructured triangular meshes. So, we developed the two-dimensional nodal S_N transport method for the neutron transport problem with triangular meshes.

In this method, the arbitrary triangle is transformed into regular one so that the transverse integration can be applied and the procedure will be simplified. The S_N quadrature set is used for describing the angular distribution of neutron flux and transverse-leakage. The orthogonal quadratic polynomial function series is used for representing the spatial distributions of neutron flux and source in the regular triangle. To achieve the accurate and efficient solution, the spatial distribution of transverse-leakage is approximated by a second-order polynomial. Using these distributions, we obtain an analytical solution for the reduced 1D transport equation. The incoming and outgoing neutron fluxes are related to the nodal average moments using this analytic solution. To achieve a stable convergence, the nodal-equivalent finite difference (NEFD) algorithm (Badruzzaman, 1985; Ikeda and Takeda, 1994) is improved for the triangular geometry. Then the Discrete Nodal Transport method for the tRiangular geometry (DNTR) is encoded. We compare our calculated results with those of some benchmark problems and could get a good agreement.

* Corresponding author. Tel.: +86 29 8266 3285; fax: +86 29 8266 7802.
E-mail address: haolianglu@gmail.com (H. Lu).

0306-4549/$ - see front matter © 2007 Elsevier Ltd. All rights reserved.
doi:10.1016/j.anucene.2007.02.004

2. Nodal S_N transport method in triangular geometry

The two-dimensional S_N transport equation in a node is written as follows:

$$\mu^m \frac{\partial \psi^{g,m}(x,y)}{\partial x} + \eta^m \frac{\partial \psi^{g,m}(x,y)}{\partial y} + \Sigma_t^g \psi^{g,m}(x,y) = Q^g(x,y) \tag{1}$$

where μ^m, η^m, components in x and y directions of neutron flight direction; m, angular direction; g, energy group; $\psi^{g,m}$, angular flux of the group g; Σ_t^g, total cross section of the group g; Q^g, neutron source given by

$$Q^g = \sum_{g'} \left\{ \sum_s^{g'-g} + \frac{\chi^g}{k_{\text{eff}}} \nu \sum_f^{g'} \right\} \phi^{g'} \tag{2}$$

Here the angular distributions of scattering and fission sources are assumed to be isotropic, and the following notation is used $\sum_s^{g'-g}$, scattering cross section (from group g' to g); k_{eff}, eigenvalue; χ^g, fission spectrum; $\nu\sum_f^{g'}$, production cross section; ϕ^g, scalar flux.

Hereafter neutron energy group g will be omitted for simplicity.

2.1. Coordinate transformation in a triangular node

Because, triangular meshes in the computational domain are arbitrary, direct application of the transverse integration would be difficult. Here, the transport equation in a regular triangular node is obtained using the coordinate transformation of Eq. (1).

We utilize the basic conception of the area coordinate which is used widely in the finite element method. For an arbitrary triangle, the Cartesian coordinates (x,y) of three vertexes will be (x_1,y_1), (x_2,y_2), (x_3,y_3) in a counter-clockwise, and the triangle area is Δ. Suppose P is a point inside the triangle and connected with three vertexes, the initial triangle is divided into three triangles Δ_1, Δ_2, Δ_3. The area coordinates λ_1, λ_2, λ_3 of P are represented by Δ_1/Δ, Δ_2/Δ, Δ_3/Δ correspondingly. Using the relation between the area coordinates λ_1, λ_2, λ_3 and the Cartesian coordinates (x,y), one can transform an arbitrary triangle in the physical coordinates into a right triangle in the area coordinates and transform this right triangle into a regular triangle (see Fig. 1) in the computational coordinates. Written in terms of the computational coordinates x' and y', the initial physical coordinates x and y will be

$$\begin{aligned} x &= (x_1+x_2+x_3)/3 + (-x_1+(x_2+x_3)/2)x' \\ &\quad + \sqrt{3}(-x_2+x_3)y'/2 \\ y &= (y_1+y_2+y_3)/3 + (-y_1+(y_2+y_3)/2)x' \\ &\quad + \sqrt{3}(-y_2+y_3)y'/2 \end{aligned} \tag{3}$$

Inserting Eq. (3) into Eq. (1), omitted the superscripts of the computational coordinates x' and y', one obtains the transformed transport equation

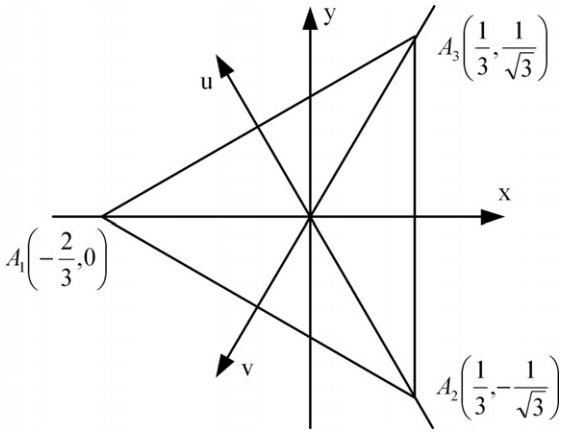

Fig. 1. Regular triangular node.

$$\mu_x^m \frac{\partial \psi^m(x,y)}{\partial x} + \eta_x^m \frac{\partial \psi^m(x,y)}{\partial y} + \Sigma_t \psi^m(x,y) = Q(x,y) \tag{4}$$

where $\mu_x^m = \frac{(-y_2+y_3)\mu^m + (x_2-x_3)\eta^m}{2\Delta}$,

$$\eta_x^m = \frac{\left(-x_1+\frac{1}{2}x_2+\frac{1}{2}x_3\right)\eta^m + \left(y_1-\frac{1}{2}y_2-\frac{1}{2}y_3\right)\mu^m}{\sqrt{3}\Delta},$$

$-2/3 \leqslant x \leqslant 1/3$, $-y_s(x) \leqslant y \leqslant y_s(x)$, $y_s(x) = (x+2/3)/\sqrt{3}$ and Δ is the area of initial arbitrary triangle.

The nodal average angular flux and three surface average angular fluxes in the physical coordinates and the computational coordinates could be proved to be equal through simple integral transformation.

2.2. Derivation of nodal transport integration equations

Integrating the transport Eq. (4) over $-y_s(x) \leqslant y \leqslant y_s(x)$ (see Fig. 1), one obtains the following 1D intra-node transport equation

$$\mu_x^m \frac{d\{y_s(x)\bar{\psi}_x^m(x)\}}{dx} + \Sigma_t y_s(x)\bar{\psi}_x^m(x) = y_s(x)\overline{Q}_x(x) - Lr_x^m(x) \tag{5}$$

where $\bar{\psi}_x^m(x)$ and $\overline{Q}_x(x)$ represent the 1D average angular flux and average neutron source within the node, respectively. $Lr_x^m(x)$ is a transverse-leakage, which is given by

$$Lr_x^m(x) = (\mu_u^m \psi_u^m(x) + \mu_v^m \psi_v^m(x))/\sqrt{3} \tag{6}$$

where $\mu_u^m = -(\mu_x^m - \sqrt{3}\eta_x^m)/2$, $\mu_v^m = -(\mu_x^m + \sqrt{3}\eta_x^m)/2$, $\psi_u^m(x) = \psi^m(x,y_s)$ and $\psi_v^m(x) = \psi^m(x,-y_s)$.

Solving Eq. (5) for the 1D average angular flux $\bar{\psi}_x^m(x)$ with $\mu_x^m > 0$, one obtains

$$y_s(x)\bar{\psi}_x^m(x) = \frac{1}{\mu_x^m}\int_{-2/3}^{x} [y_s(x')\overline{Q}_x(x') - Lr_x^m(x')] e^{-\frac{\Sigma_t}{\mu_x^m}(x-x')} dx' \tag{7}$$

and the outgoing surface average flux at the right ($x = 1/3$) will be

$$\bar{\psi}_x^m = \frac{\sqrt{3}}{\mu_x^m}\int_{-2/3}^{1/3} \left[y_s(x)\overline{Q}_x(x) - Lr_x^m(x)\right] e^{-\frac{\Sigma_t}{\mu_x^m}(1/3-x)} dx \tag{8}$$

An analogous equation for $\mu_x^m < 0$ can be derived

$$y_s(x)\bar{\psi}_x^m(x) = \frac{1}{|\mu_x^m|}\int_x^{1/3}\left[y_s(x')\overline{Q}_x(x') - Lr_x^m(x')\right]e^{-\frac{\Sigma_t}{|\mu_x^m|}(x'-x)}dx' + \frac{\sqrt{3}}{3}e^{-\frac{\Sigma_t}{|\mu_x^m|}(1/3-x)}\bar{\psi}_x^m \quad (9)$$

Because, there is a vertex (see Fig. 1) and $y_s(x)\bar{\psi}_x^m(x) = 0$ at the left side ($x = -2/3$) of the regular triangular node, we only need to consider the surface average angular flux at the right side in the x direction.

2.3. Flux, source and transverse-leakage approximations

Eqs. (7)–(9) are the exact analytical solutions in the x direction in the transverse-integrated nodal method. The integrals arising in these equations are evaluated by approximating the spatial variations of the node-interior average angular flux, average source and transverse-leakage. In the discrete nodal transport method (DNTM), the node-interior average angular flux is usually expanded in terms of Legendre polynomials. Here, their spatial dependence is represented by a quadratic polynomial expansion as

$$\bar{\psi}_x^m(x) = \sum_{i=0}^{2}\bar{\psi}_{xi}^m h_i(x) \quad (10)$$

$$\overline{Q}_x(x) = \sum_{i=0}^{2}\overline{Q}_{xi}h_i(x) \quad (11)$$

where $h_i(x) = \{1, x, x^2 + 2x/15 - 1/18\}$, and the polynomials $h_i(x)$ form an orthogonal set with respect to the weight function $y_s(x)$

$$\int_{-2/3}^{1/3} y_s(x)h_i(x)h_j(x)dx = 0, \quad \text{for } i \neq j \quad (12)$$

This polynomial expansion technique allows us to treat the multi-group formulation with reasonable accuracy.

The biggest difficulty of the nodal transport method in a triangular geometry is the spatial modeling of a transverse-leakage with high-leakage. In the original DNTM, a flat approximation is used for the spatial distribution of transverse-leakage and calculated accurately even in case of the large mesh widths.

We developed a new spatial model for transverse-leakage in the nodal method to describe the accurate spatial distribution. The spatial distribution of the node-interior flux is approximated by a binary quadratic polynomial expansion in the computational coordinates

$$\psi^m(x,y) = a(x^2+y^2) + bx + cy + d \quad (13)$$

The coefficients a, b, c, d can be derived from the values of three surface average angular fluxes $\bar{\psi}_x^m$, $\bar{\psi}_u^m$, $\bar{\psi}_v^m$ and the nodal averaged angular flux $\bar{\psi}^m$. Inserting the coordinate values of three vertexes (see Fig. 1) into Eq. (13), one obtains three corner-point fluxes

$$\begin{aligned}\psi_{px}^m &= 5(\bar{\psi}_u^m + \bar{\psi}_v^m)/3 - \bar{\psi}_x^m/3 - 2\bar{\psi}^m\\ \psi_{pu}^m &= 5(\bar{\psi}_v^m + \bar{\psi}_x^m)/3 - \bar{\psi}_u^m/3 - 2\bar{\psi}^m\\ \psi_{pv}^m &= 5(\bar{\psi}_x^m + \bar{\psi}_u^m)/3 - \bar{\psi}_v^m/3 - 2\bar{\psi}^m\end{aligned} \quad (14)$$

Using ψ_{px}^m, ψ_{pv}^m, $\bar{\psi}_u^m$ and ψ_{px}^m, ψ_{pu}^m, $\bar{\psi}_v^m$, two quadratic polynomials of $\psi_u^m(x)$ and $\psi_v^m(x)$ are constructed, respectively. Then the spatial distribution of transverse-leakage (see Eq. (6)) is expressed by

$$Lr_x^m(x) = (Lr_{x0}^m + Lr_{x1}^m x + Lr_{x2}^m x^2)/\sqrt{3} \quad (15)$$

where

$$\begin{aligned}Lr_{x0}^m &= \frac{1}{3}\mu_u(4\bar{\psi}_u^m - \psi_{px}^m) + \frac{1}{3}\mu_v(4\bar{\psi}_v^m - \psi_{px}^m)\\ Lr_{x1}^m &= 2\mu_u(\psi_{pv}^m - \bar{\psi}_u^m) + 2\mu_v(\psi_{pu}^m - \bar{\psi}_v^m)\\ Lr_{x2}^m &= 3\mu_u(\psi_{px}^m + \psi_{pv}^m - 2\bar{\psi}_u^m) + 3\mu_v(\psi_{px}^m + \psi_{pu}^m - 2\bar{\psi}_v^m)\end{aligned}$$

Inserting Eqs. (10), (11) and (15) into Eq. (8), one obtains

$$\bar{\psi}_x^m = \sum_{i=0}^{2}P_{xi}^m\overline{Q}_{xi} + \sum_{i=0}^{2}R_{xi}^m Lr_{xi}^m \quad (16)$$

where $P_{xi}^m = \frac{\sqrt{3}}{\mu_x^m}\int_{-2/3}^{1/3} y_s(x)h_i(x)e^{-\frac{\Sigma_t}{\mu_x^m}(1/3-x)}dx$ and $R_{xi}^m = -\frac{\sqrt{3}}{\mu_x^m}\int_{-2/3}^{1/3} x^i e^{-\frac{\Sigma_t}{\mu_x^m}(1/3-x)}dx$.

Inserting Eqs. (10), (11) and (15) into Eq. (7) and applying the weighted residual method to Eq. (7), one obtains the average angular flux moments $\bar{\psi}_{xi}^m$ for $\mu_x^m > 0$

$$\bar{\psi}_{x0}^m = \sum_{j=0}^{2}\left(F_{x0j}^m\overline{Q}_{xj} + G_{x0j}^m Lr_{xj}^m\right) \quad (17a)$$

$$\bar{\psi}_{xi}^m = \sum_{j=0}^{2}\left(F_{xij}^m\overline{Q}_{xj} + G_{xij}^m Lr_{xj}^m\right), \quad \text{for } i = 1,2 \quad (17b)$$

where $F_{xij}^m = \frac{1}{\mu_x^m D_i}\int_{-2/3}^{1/3} h_i(x)dx\int_{-2/3}^{x} y_s(x')h_j(x')e^{-\frac{\Sigma_t}{\mu_x^m}(x-x')}dx'$, $G_{xij}^m = -\frac{1}{\mu_x^m D_i}\int_{-2/3}^{1/3} h_i(x)dx\int_{-2/3}^{x}(x')^j e^{-\frac{\Sigma_t}{\mu_x^m}(x-x')}dx'$ and $D_i = \int_{-2/3}^{1/3} y_s(x)\{h_i(x)\}^2dx$.

Similar substitutions into Eq. (9), the nodal interior average angular flux moments for $\mu_x^m < 0$ can be derived

$$\bar{\psi}_{x0}^m = \sum_{j=0}^{2}(F_{x0j}^m\overline{Q}_{xj} + G_{x0j}^m Lr_{xj}^m) + H_{x0}^m\bar{\psi}_x^m \quad (18a)$$

$$\bar{\psi}_{xi}^m = \sum_{j=0}^{2}(F_{xij}^m\overline{Q}_{xj} + G_{xij}^m Lr_{xj}^m) + H_{xi}^m\bar{\psi}_x^m, \quad \text{for } i = 1,2 \quad (18b)$$

where $F_{xij}^m = \frac{1}{|\mu_x^m|D_i}\int_{-2/3}^{1/3} h_i(x)dx\int_{x}^{1/3} y_s(x')h_j(x')e^{-\frac{\Sigma_t}{|\mu_x^m|}(x'-x)}dx'$, $G_{xij}^m = -\frac{1}{|\mu_x^m|D_i}\int_{-2/3}^{1/3} h_i(x)dx\int_{x}^{1/3}(x')^j e^{-\frac{\Sigma_t}{|\mu_x^m|}(x'-x)}dx'$, $H_{xi}^m = \frac{1}{\sqrt{3}D_i}\int_{-2/3}^{1/3} h_i(x)e^{-\frac{\Sigma_t}{|\mu_x^m|}(1/3-x)}dx$ and $D_i = \int_{-2/3}^{1/3} y_s(x)\{h_i(x)\}^2dx$.

Integration of the average angular flux moments over angle yields

$$\bar{\phi}_{xi} = \sum_m \omega^m \bar{\psi}^m_{xi} \tag{19}$$

where ω^m is a weight of the angular quadrature set. Furthermore, the source moments Q_i are calculated by

$$\overline{Q}^g_{xi} = \sum_{g'} \left\{ \sum_s^{g'-g} + \frac{\chi^g}{k_{\text{eff}}} \nu \sum_f^{g'} \right\} \bar{\phi}^{g'}_{xi} \tag{20}$$

By the same procedure described above, the analogous nodal coupling equations corresponding to the u and v directions are derived, and $\bar{\psi}^m_u$, $\bar{\psi}^m_v$, $\bar{\psi}^m_{ui}$, $\bar{\psi}^m_{vi}$, $\overline{Q}_{ui}$ and $\overline{Q}_{vi}$ are calculated.

Thus we have derived the nodal coupling equations and the average angular flux moments corresponding to the x, u, v directions. The nodal S_N transport equation is calculated as follows: the average angular fluxes at the incoming surfaces are first assumed and then the 0th-order average angular flux moments in the intra-node and the average angular fluxes at the outgoing surface are calculated. The average angular fluxes at the outgoing surfaces are used as the average angular fluxes at the incoming surfaces of the next adjacent node. The nodal averaged angular fluxes are calculated by averaging three 0th-order average angular flux moments calculated in the x, u and v directions.

3. NEFD algorithm and its improvement

The standard algorithm of the nodal S_N transport method described in Section 2.3, requires a lot of memories of the computer with increase of the mesh number and thus impractical. The nodal-equivalent finite difference (NEFD) method (Badruzzaman, 1985; Ikeda and Takeda, 1994) reduces the computational time and the required memory, while retaining the accuracy over the standard S_N method. The NEFD algorithm has same advantages for the triangular geometry.

Sweeping from the initial physical domain in the direction of the angle Ω^m, seen in Fig. 2, there are two incoming surfaces in a triangle 1, while one incoming surface in a triangle 2. Here, the NEFD algorithm would be used in case of two surfaces of a triangle being incoming surfaces as described in Section 3.1, while the improved NEFD algorithm is employed when one surface of a triangle is an incoming surface and this case is described in Section 3.2.

3.1. NEFD algorithm in case of two incoming surfaces

In the NEFD algorithm, Eqs. (16)–(18) are reformulated. Let us consider the surface flux in the x direction being unknown, one obtains the following equation by eliminating $\overline{Q}_{x0}$ from Eqs. (16) and (17a)

$$\bar{\psi}^m_x = \alpha^m_x \bar{\psi}^m + \beta^m_x \tag{21}$$

where $\alpha^m_x = \frac{P^m_{x0}}{F^m_{x00}}$ and $\beta^m_x = \sum_{i=1}^2 (P^m_{xi} - F^m_{x0i}\alpha^m_x)\overline{Q}_{xi} + \sum_{i=0}^2 (R^m_{xi} - G^m_{x0i}\alpha^m_x) Lr^m_{xi}$.

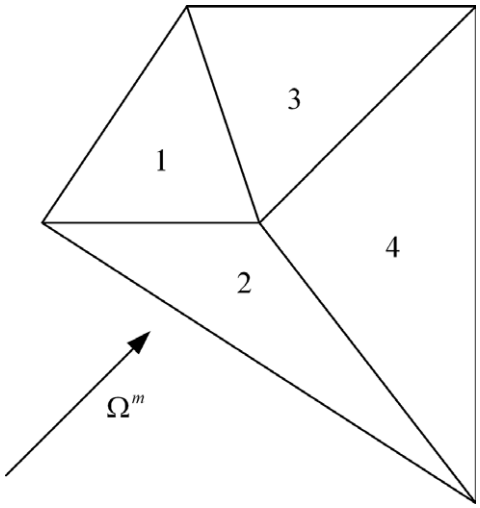

Fig. 2. Sweeping of triangular meshes.

The neutron balance equation in a regular triangle is

$$2\mu^m_x \bar{\psi}^m_x + 2\mu^m_u \bar{\psi}^m_u + 2\mu^m_v \bar{\psi}^m_v + \Sigma_t \bar{\psi}^m = \overline{Q} \tag{22}$$

Substituting Eq. (21) into Eq. (22), one obtains the nodal averaged flux

$$\bar{\psi}^m = \frac{\overline{Q} - 2\mu^m_x \beta^m_x - 2\mu^m_u \bar{\psi}^n_u - 2\mu^m_v \bar{\psi}^m_v}{\Sigma_t + 2\mu^m_x \alpha^m_x} \tag{23}$$

Here, $\bar{\psi}^m$ involves only the previous-iteration source moments and the incoming surface average fluxes.

Eliminating $\overline{Q}_{x0}$ from Eqs. (17a) and (17b), one obtains the high-order average flux moments for $\mu^m_x > 0$

$$\bar{\psi}^m_{xi} = u^m_{xi} \bar{\psi}^m + v^m_{xi}, \quad \text{for } i = 1, 2 \tag{24}$$

where $u^m_{xi} = \frac{F^m_{xi0}}{F^m_{x00}}$, $v^m_{xi} = \sum_{j=1}^2 (F^m_{xij} - F^m_{x0j} u^m_{xi})\overline{Q}_{xj} + \sum_{j=0}^2 \times (G^m_{xij} - G^m_{x0j} u^m_{xi}) Lr^m_{xj}$.

Similar equations for $\mu^m_x < 0$ can be obtained by eliminating $\overline{Q}_{x0}$ from Eq. (18a) and (18b)

$$\bar{\psi}^m_{xi} = u^m_{xi} \bar{\psi}^m + v^m_{xi} + w^m_{xi} \bar{\psi}^m_x, \quad \text{for } i = 1, 2 \tag{25}$$

where the expressions of u^m_{xi} and v^m_{xi} are the same as those in Eq. (24) and $w^m_{xi} = H^m_{xi} - u^m_{xi} H^m_{x0}$.

In the present NEFD algorithm, the nodal averaged angular flux is obtained from Eq. (23). And then using the updated nodal averaged angular flux, the average angular flux at the outgoing surface and high-order average angular flux moments in the x, u, v directions are calculated from Eqs. (21), (24) and (25).

3.2. Improved NEFD algorithm in case of one incoming surface

In Fig. 2, the direction in the angle of Ω^m is paralleled with the common edge between the triangle 3 and triangle 4. According to the expression of μ^m_x defined in Eq. (4), the component in the direction of the angle Ω^m is zero in the

common edge. In the computation, we take the component in the common edge of the triangle 3 being -10^{-7}, and 10^{-7} in that of the triangle 4. Here, 10^{-7} means a sufficiently small number. The triangle 3 has two incoming surfaces and thus the NEFD algorithm could be used. In the triangle 4, only one surface is an incoming surface and the NEFD algorithm does not converge with decrease of the mesh width.

Consider the triangle 4, we transform it into a regular triangle in the computation coordinates (see Fig. 3) and suppose that $\bar{\psi}_x^m$ and $\bar{\psi}_u^m$ are unknown and $\mu_u^m = 10^{-7}$. Then the corner-point fluxes ψ_{px}^m, ψ_{pu}^m and the surface average angular flux $\bar{\psi}_v^m$ are given by the previous calculations at two adjacent nodes, and $\mu_x^m = -\mu_v^m$. In the u direction, the Eq. (21) will be

$$\bar{\psi}_u^m = \left(\sum_t \bar{\psi}^m + \overline{Q}_{u1}/3 + \overline{Q}_{u2}/10 + Lr_{u0}^m - 2Lr_{u1}^m/3 + Lr_{u2}^m/9 \right) \Big/ \Sigma_t \tag{26}$$

Ignoring the high-order average source moments and inserting Eqs. (14) and (15) into Eq. (26), yields

$$\bar{\psi}_u^m = A\bar{\psi}_u^m + C \tag{27}$$

where $A = 5\mu_v^m/(3\Sigma_t)$, $C = (\Sigma_t\bar{\psi}^m + \mu_v^m(5\bar{\psi}_v^m/3 - \bar{\psi}_x^m/3 - 2\bar{\psi}^m - \psi_{px}^m))/\Sigma_t$ and $\mu_v^m = ((y_2 - y_1)\mu^m + (x_1 - x_2)\eta^m)/2\Delta$. For $\mu_u^m = 10^{-7}$, $\bar{\psi}^m$ and $\bar{\psi}_x^m$ can be calculated accurately through Eqs. (15), (21) and (23), and then C is given. Suppose Δx is mesh width, $y_2 - y_1 = \Delta x$, $x_1 - x_2 = \Delta x$, $\Delta = \Delta x^2/2$ and $\mu^m = \eta^m$, and then $\mu_v^m = 2\mu^m/\Delta x$ and $A = 10\mu^m/(3\Delta x\Sigma_t)$. The Eq. (27) converges only for $|A| < 1$. So we can derive $\Delta x > 10|\mu^m|/(3\Sigma_t)$. In other words, the iteration of Eq. (27) would not converge when the mesh width is less than 3.3 mean free paths.

In order to converge the iteration, the improved NEFD algorithm is used when one surface of a triangle is an incoming surface. The average angular fluxes at the two outgoing surfaces are expressed in terms of the nodal averaged angular flux, higher order average source moments, the average angular flux at the incoming surface, and two known corner-point fluxes through the insertion of Eqs. (14) and (15) into Eq. (21). Addition of Eq. (22) to the equations for two outgoing surfaces resulted above, the set of ternary linear equations is given and the average angular fluxes at the two outgoing surfaces and the nodal averaged angular flux could be obtained. Analogously, the average angular flux moments of high-order in the x, u, v directions are calculated using the updated nodal averaged angular flux and two updated average angular fluxes at the outgoing surfaces from Eqs. (24) and (25) shown in Section 3.1.

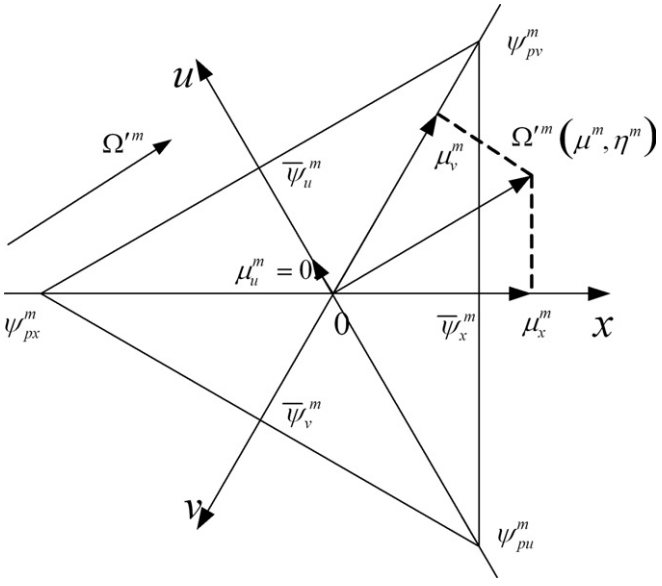

Fig. 3. Regular triangle in case of one incoming surface.

4. Numerical results

The discrete nodal transport method for a 2D triangular geometry (DNTR) developed in the paper has been applied successfully to a number of benchmark problems. For checking its computational accuracy and efficiency, the four problems were solved. The capability of this method for the unstructured geometry was investigated applying it to the fifth benchmark problem. Finally, a benchmark problem with hexagonal assemblies was solved.

4.1. Calculation of k_{eff} in a homogeneous slab

This benchmark problem of a slab with one-energy group and vacuum boundary conditions was solved by Stepanek (1981) in which the thickness of the slab is given to be 10 cm. To simulate the infinite extension of the slab in the y direction, 10 cm width and reflective boundary conditions are used. In the DNTR code, the triangular meshes are obtained by dividing a rectangular mesh used in the DNTM code into two triangular meshes.

The eigenvalues as a function of the mesh width calculated by the four kinds of methods are shown in Table 1

Table 1
Eigenvalue for homogeneous slab

N[a]	K[a]	ANISN		DNTM		DNTR		DOT4.2	
		k_{eff}	K[a]	k_{eff}	CPU time/s	k_{eff}	CPU time/s	k_{eff}	CPU time/s
4	5	0.94178	2	0.95184	0.03	0.94569	0.03	–	–
	10	0.94956	5	0.95192	0.25	0.95126	0.08		
	20	0.95147	10	0.95192	0.98	0.95180	0.34		
	40	0.95194	20	0.95192	3.94	0.95190	1.36		
8	5	0.94280	2	0.95300	0.12	0.94707	0.06	–	–
	10	0.95068	5	0.95308	0.80	0.95249	0.27	0.94236	0.44
	20	0.95257	10	0.95309	3.20	0.95296	1.06	0.95019	0.50
	40	0.95303	20	0.95309	13.12	0.95302	4.23	0.95208	1.88
Reference		0.95348							

[a] N means the order of angular quadrature set and K is the number of meshes in the x direction.

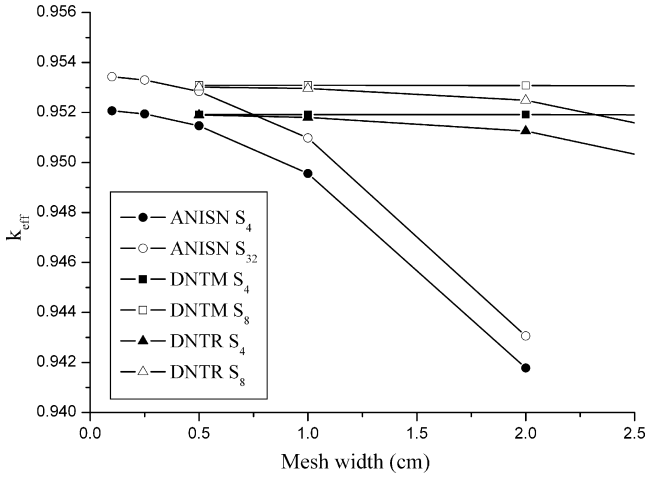

Fig. 4. Calculated eigenvalues and their dependence on mesh width.

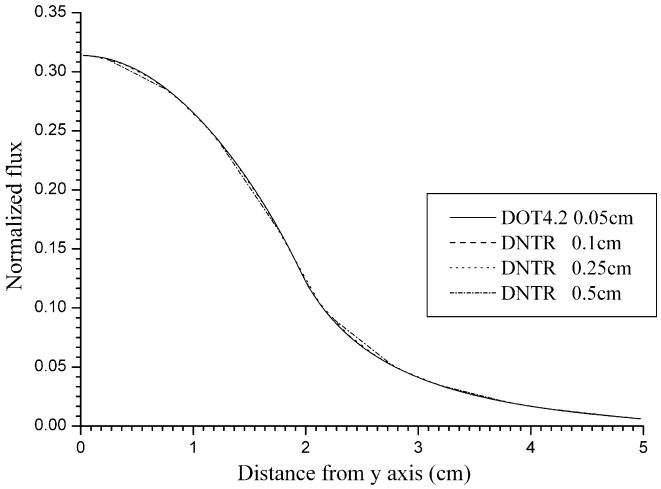

Fig. 6. Flux distribution along the x axis.

and Fig. 4, and also their execution times are shown in Table 1. The results of the ANISN code are taken from Stepanek (1981). From Table 1 and Fig. 4, it can be seen that the DNTR code converges more speedily than other codes. Even if the mesh width of four times larger than that of the ANISN and DOT4.2 codes is used in the DNTR code, the same eigenvalue of 0.9525 is obtained, and the execution time of the DNTR code is just one-seventh of the DOT4.2 code. And even the mesh numbers in the DNTR code are twice than those of the DNTM code, but with same mesh width, the execution time is still less than the DNTM code because the iterative scheme of the DNTR code reduces the required memories and computational times significantly.

4.2. Issa test problem

This benchmark problem is a one-group two-region system, and the cross-sections are given by Issa et al. (1986). Fig. 5 gives the geometry of the problem. Only the right side has a vacuum condition while the other sides are reflecting boundary conditions. The triangular meshes used in the DNTR code are obtained by dividing a rectangular mesh used in the DOT4.2 code into two triangular meshes.

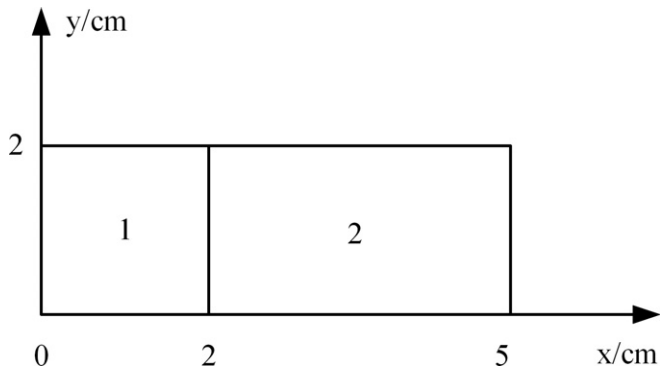

Fig. 5. Geometry of Issa benchmark problem.

Table 2
Comparison of results for the Issa problem

Method	DNTR	DNTR	DNTR	DOT4.2
Mesh widths (cm)	0.1	0.25	0.5	0.05
k_{eff}	1.678047	1.678043	1.678023	1.67790
CPU time (s)	5.422	0.797	0.234	15.797

Conventional S_8 angular quadrature is selected in this problem.

The distributions of flux along the x axis, calculated by the DNTR and DOT 4.2 codes with different mesh widths, are shown in Fig. 6. In the figure, the fluxes are normalized so that $\int \nu\Sigma_f \Phi dV = 1$. From Fig. 6, the calculated results with different mesh widths by the DNTR code agree well with that of the DOT4.2 code, even the mesh width is ten times larger than that of the DOT4.2 code. The reference eigenvalue is 1.6784. In Table 2, the calculated eigenvalues and execution times in two codes are compared, in which the same precision of the eigenvalue is obtained in both

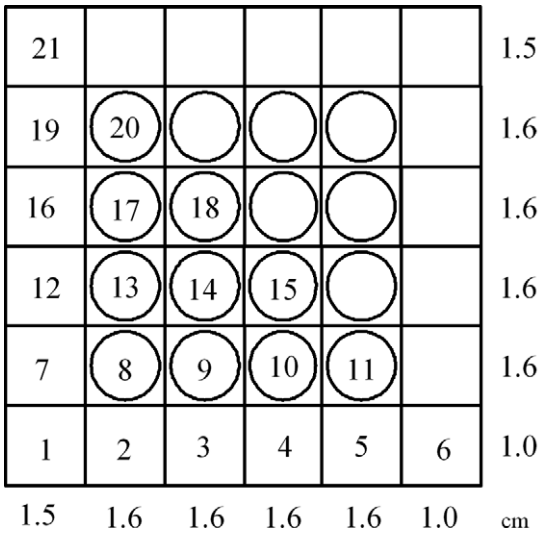

Fig. 7. Geometry of LWR assembly.

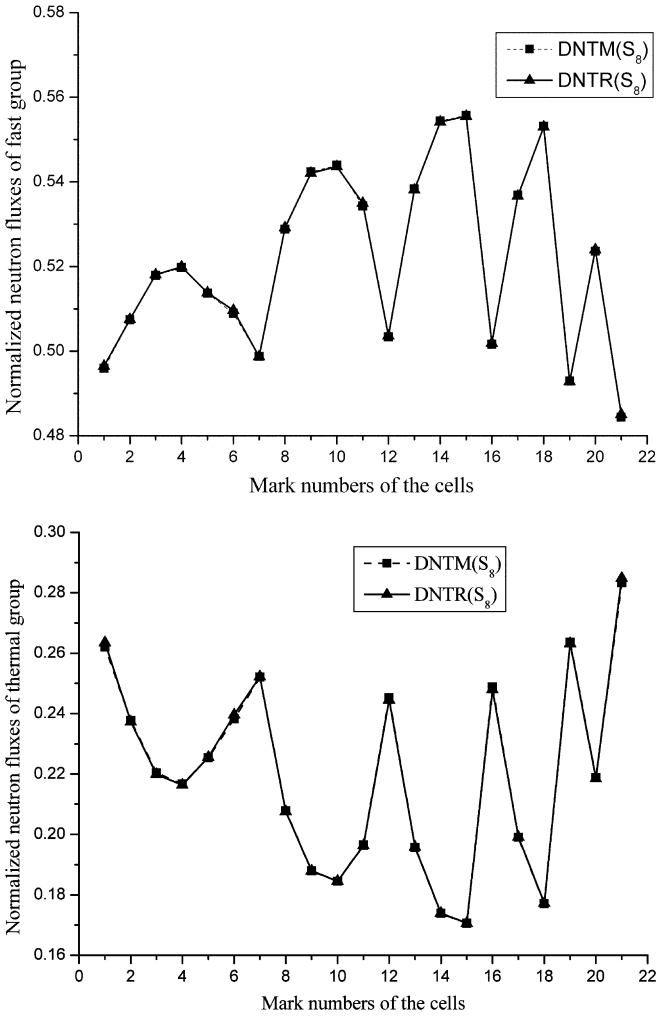

Fig. 8. The neutron fluxes and their dependence on the mark numbers of the cells.

cases, but the execution time of the DNTR code is 20 times shorter than the case of the DOT4.2 code when the mesh width of DNTR is 0.25 cm.

4.3. 4 × 4 LWR assembly

The LWR fuel assembly with 25 cells (see Fig. 7) and reflection boundary conditions is treated using the conventional S_8 angular quadrature and the cross sections given by Stepanek et al. (1983). The triangular meshes used in the DNTR code are obtained by dividing a rectangular mesh used in the DNTM code into two triangular meshes.

The eigenvalues obtained by the DNTR and DNTM codes are 1.212519 and 1.212703, respectively. The relative

Table 3
Comparison of results for IAEA benchmark problem

Method	Average fluxes in various regions[a]					k_{eff}	CPU time/s
	Zone 1	Zone 2	Zone 3	Zone 4	Zone 5		
SURCU	0.01686	0.000125	0.000041	0.000295	0.000791	1.0083	–
FELICIT	0.01685	0.000127	0.000042	0.000300	0.000797	1.0069	–
TEPFEM	0.01686	0.000125	0.000033	0.000297	0.000784	1.0079	115.438
DOT4.2	0.01686	0.000124	0.000037	0.000294	0.000789	1.0088	126.922
DNTR	0.01686	0.000125	0.000035	0.000295	0.000791	1.0085	22.953

[a] The fluxes are normalized so that $\int \nu\Sigma_f \Phi dV = 1$.

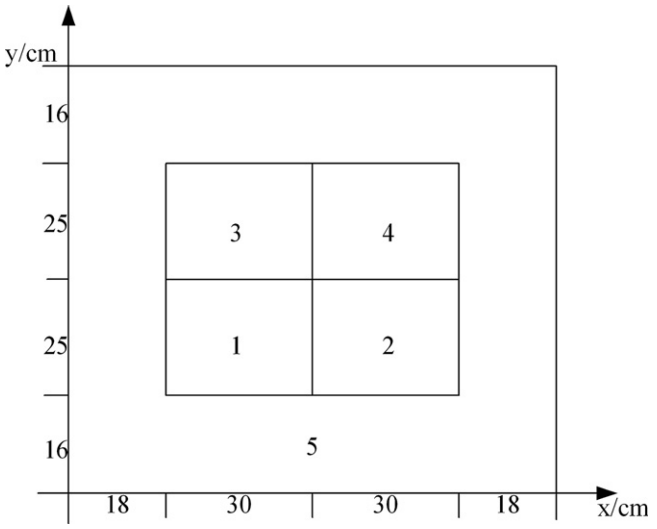

Fig. 9. Geometry of IAEA benchmark problem.

Table 4
Results of the unstructured mesh problem

Method	The fluxes of fast neutron		The fluxes of thermal neutron		k_{eff}
	Fuel[a]	Water	Fuel	Water	
MG-MCNP3B	1.0	1.80023	0.55211	1.08581	1.174655
TEPFEM	1.0	1.82777	0.55749	1.10730	1.171747
DNTR	1.0	1.82734	0.55759	1.10504	1.174551

[a] Normalization: the fast flux in fuel zone is 1.0.

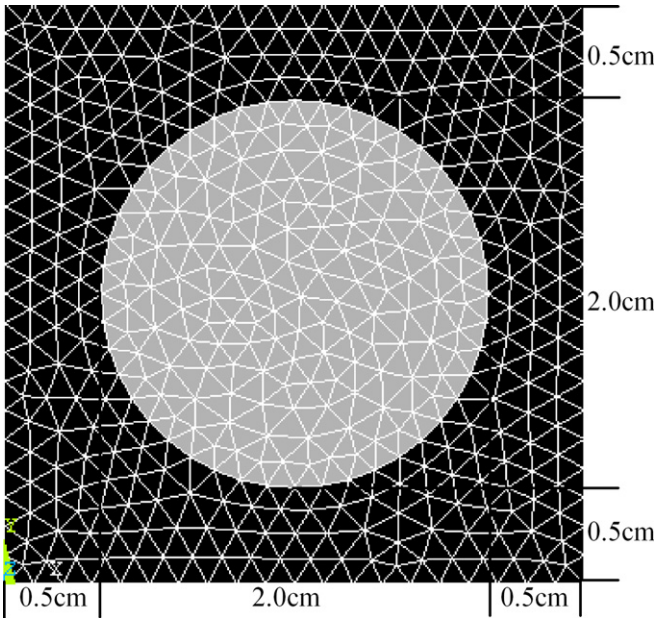

Fig. 10. Unstructured mesh.

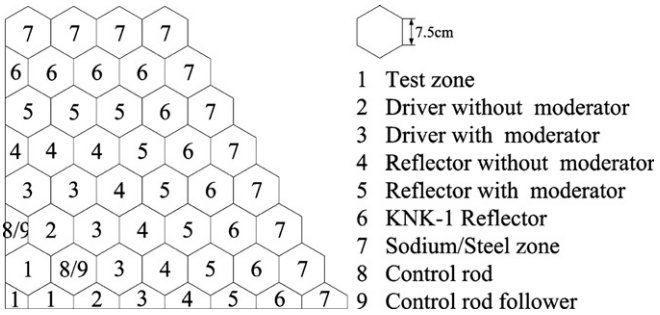

Fig. 11. 2D-KNK benchmark problem.

error is −0.015%. Corresponding execution times of two codes are 0.91 s and 1.80 s. The DNTR code is still faster than the DNTM code. The fluxes and their dependence on the mark numbers of the cell are illustrated in Fig. 8, in which the abscissa axis is the mark number of the cell. The flux is normalized by $\int \nu\Sigma_f \Phi \mathrm{d}V = 1$. The maximum relative error in all labeled cells is 0.572%. It can be found this code has the same precision with the DNTM code.

4.4. IAEA light water reactor

The simplified reactor with the vacuum boundary conditions, consisting of two large source zones and two large absorber zones surrounded by the light water (see Fig. 8), is treated in which we use the conventional S_4 angular quadrature and unstructured triangular meshes with the size and shape in random.

Results are compared in Table 3, in which the TEPFEM (Cao and Wu, 2004) code of a finite element spherical-harmonics method was also applied to the unstructured meshes. Here, the angular variable of the TEPFEM code is expanded by P_3. The mesh widths of the TEPFEM, DOT4.2 and DNTR codes are 4 cm, 1 cm and 4 cm, respectively. From Table 3, the results calculated by the DNTR code are in a good agreement with the other four codes, and execution times of the DOT4.2 and TEPFEM codes are about 5 times longer than that of the DNTR code.

4.5. Problem with unstructured meshes

A problem with non-regular geometry (Cao and Wu, 2004) is adopted to confirm the capability of the DNTR code to the unstructured triangular meshes. It contains a fuel rod surrounded by the light water as shown in Fig. 9. The cross sections are the same with the LWR assembly problem in Section 4.3. Conventional S_6 angular quadrature is used for this problem. The mesh width of the DNTR code is 0.15 cm.

Table 4 summarizes results obtained by various codes. The results of the DNTR code show a good agreement

Table 5
Percentage errors of the region-averaged group fluxes for the 2D KNK benchmark problem

Region	Rods-in			Rods-out		
	Reference (TWOHEX-96Δ)	TWOHEX-6Δ	DNTR S_4	Reference (TWOHEX-96Δ)	TWOHEX-6Δ	DNTR S_4
Group 1						
Test zone	3.90232E−02	0.48	0.19	3.13200E−02	0.11	0.19
Driver without moderator	2.63616E−02	0.09	−0.07	2.33354E−02	−0.02	−0.17
Driver with moderator	1.80327E−02	0.22	−0.17	1.53025E−02	−0.06	−0.04
Reflector without moderator	7.38592E−03	0.94	0.32	6.03135E−03	0.37	0.29
Control rod	2.34097E−02	1.01	−0.37	–	–	–
Control rod follower	–	–	–	2.32517E−02	0.28	−0.32
Group 2						
Test zone	2.86349E−02	0.24	0.11	2.70066E−02	0.08	0.05
Driver without moderator	1.91338E−02	−0.17	−0.03	1.99348E−02	−0.20	−0.20
Driver with moderator	1.27865E−02	0.25	−0.10	1.22778E−02	0.10	0.01
Reflector without moderator	7.13720E−03	−0.04	−0.07	6.23672E−03	−0.54	−0.02
Control rod	1.71486E−02	1.14	−0.12	–	–	–
Control rod follower	–	–	–	2.14954E−02	0.10	−0.06
Group 3						
Test zone	4.94818E−03	−0.76	0.22	7.57104E−03	0.03	−0.08
Driver without moderator	5.05859E−03	−0.47	−0.06	7.36266E−03	0.52	0.02
Driver with moderator	6.69590E−03	−0.13	−0.13	7.00912E−03	−0.07	−0.01
Reflector without moderator	4.58171E−03	0.16	−0.11	4.16147E−03	−0.48	−0.06
Control rod	3.11700E−03	1.98	−0.10	–	–	–
Control rod follower	–	–	–	8.43477E−03	−0.24	−0.02
Group 4						
Test zone	1.57957E−04	−4.10	1.43	7.97467E−04	−0.80	−0.45
Driver without moderator	8.75407E−04	−0.37	−0.02	1.55391E−03	2.39	0.27
Driver with moderator	3.32370E−03	−0.51	−0.04	3.55912E−03	−0.44	0.00
Reflector without moderator	4.97038E−03	0.84	0.19	4.50078E−03	0.23	0.27
Control rod	1.88818E−04	3.79	−1.07	–	–	–
Control rod follower	–	–	–	2.40342E−03	−2.68	−0.10
K_{eff} ε_k (%)	1.00941	−0.482	−0.027	1.30945	−0.096	−0.047

with the reference results, and verify that the DNTR code is more efficient in solving the transport problem of the non-regular geometry.

4.6. 2D KNK benchmark problem

The KNK problem is a four-group, eight-ring fast breeder reactor (FBR) with 169 assemblies (Kim and Cho, 1996). The layout of this reactor problem is shown in Fig. 10. Two configurations have been studied, which control rods out and in. Vacuum boundary conditions are applied at all outer boundaries of the problem and S_4 angular quadrature is used. The triangular meshes used in the DNTR code are obtained by dividing a hexagonal mesh into six triangular meshes (Fig. 11).

Table 5 shows the results of region-averaged group fluxes and k_{eff} comparisons of TWOHEX-96Δ , TWOHEX-6Δ and the present method. The fluxes are normalized so that $\int v\Sigma_f \Phi \mathrm{d}V = 1$. The eigenvalues of DNTR agree well with the reference in both cases, with the difference being less than 0.05% Δk. On the other hand, the difference of TWOHEX-6Δ is -0.482% Δk in the rods-in case. From Table 5, the results of region-averaged group fluxes are also better than those of TWOHEX-6Δ.

5. Conclusions

The advanced nodal method for the solution of the multi-group neutron transport equation in two-dimensional triangular geometry is developed and evaluated. Before the transverse integration is applied, we transform the arbitrary triangles into regular triangles using coordinate transformation. In the regular triangular node, the equations of the x, u, v directions can be derived analogously and the nodal average angular flux and three surface average angular fluxes are equaled with those of the arbitrary triangular node. The angular distributions of intra-node neutron fluxes and its transverse-leakage are represented by the S_N quadrature set. The spatial distributions of neutron flux and source in a regular triangle are given approximately by an orthogonal binary quadratic polynomial, and the spatial expansion of transverse-leakage is approximated by a second-order polynomial. To establish a stable and efficient iterative scheme, the improved nodal-equivalent finite difference algorithm is used.

The nodal method is applied to several two-dimensional benchmark problems. The results demonstrate the higher capability of the method to yield the very accurate results in smaller computing times than those required by the standard finite difference method and the finite element spherical-harmonics method.

Acknowledgements

The authors acknowledge Prof. Takeshi KAWAI of Xi'an Jiaotong University for his helpful remarks. This work is supported by National Natural Science Foundation of China Grants No. 10475064 and National Key Laboratory of Reactor System Design Technology Grants No. SYX-01-05-09.

References

Badruzzaman, A., 1985. An efficient algorithm for nodal-transport solutions in multidimensional geometry. Nucl. Sci. Eng. 89 (3), 281–290.

Cao, L.Z., Wu, H.C., 2004. Spherical harmonics method for neutron transport equation based on unstructured-meshes. Nucl. Sci. Tech. 15 (6), 335–339.

Ikeda, H., Takeda, T., 1994. A new nodal S_N transport method for three-dimensional hexagonal geometry. J. Nucl. Sci. Technol. 31 (6), 497–509.

Issa, J.G., Riyait, N.S., Goddard, A.J.H., et al., 1986. Multigroup application of the anisotropic FEM code FELTRAN to one, two, three-dimensional and R-Z problems. Prog. Nucl. Energy 18 (1), 251–264.

Kim, C.H., Cho, J.Y., 1996. Source projection analytic nodal SN method for hexagonal geometry. Ann. Nucl. Energy 23 (2), 133–143.

Mathews, K.A., Brennan, C.R., 1997. Exponential characteristic nonlinear radiation transport method for unstructured grids of triangular cells. Nucl. Sci. Eng. 126, 264–281.

McGhee, J.M., Roberts, R.M., Morel, J.E., 1997. The DANTE Boltzmann transport solve: an unstructured mesh, 3D, spherical harmonics algorithm compatible with parallel computer architectures. In: Proceedings of Joint International Conference on Mathematical Methods and Supercomputing in Nuclear Applications, 5–10 October 1997, Saratoga Springs, New York, America.

Ressel, K.J., Starke, G., 2000. A boundary functional for the least-squares finite-element solution of neutron transport problems. SIAM J. Numer. Anal. 37 (2), 556–586.

Stepanek, J., 1981. The DP_N surface flow integral neutron transport method for slab geometry. Nucl. Sci. Eng. 78 (1), 53–65.

Stepanek, J., Auerbach, T., Haelg, W., 1983. Calculation of four thermal reactor benchmark problems in X–Y geometry, EPRI NP-2855.

Wagner, M.R., 1989. Three-dimensional nodal diffusion and transport theory methods for hexagonal-z geometry. Nucl. Sci. Eng. 103 (4), 377–391.